

# An iterative implementation of rotated coordinates for inverse problems

Tracianne B. Neilsen

*Applied Research Laboratories, The University of Texas at Austin, P.O. Box 8029, Austin, Texas 78713-8029*

(Received 3 May 2002; revised 18 October 2002; accepted 24 January 2003)

A generalized inversion method is presented that uses a rotated coordinates technique [Collins and Fishman, *J. Acoust. Soc. Am.* **98**, 1637–1644 (1995)] in simulated annealing to invert for both the location of an acoustic source and parameters that describe the ocean seabed. The rotated coordinates technique not only aids in the inversion process but also indicates the coupling of the source and environmental parameters and the relative sensitivities of the cost function to changes in the various parameters. The information obtained from the rotated coordinates provides insights into how the inversion problem can be effectively decoupled. An iterative process consisting of multiple simulated annealing runs that each use a different set of rotated coordinates is demonstrated. This multistep algorithm is called systematic decoupling using rotated coordinates and is especially helpful when inverting for a large number of unknown parameters. The cost function minimized in the inversion algorithm is model-data cross-hydrophone spectra summed coherently over frequency and receiver pairs. The results of applying this inversion method to simulated data are presented in this paper. © 2003 Acoustical Society of America. [DOI: 10.1121/1.1562912]

PACS numbers: 43.30.Pc [WLS]

## I. INTRODUCTION

An iterative, efficient generalized inversion scheme to obtain the location of an acoustic source and the characteristics of the ocean environment is presented. The primary goals of the method are to minimize the number of *a priori* decisions and the number of forward calls required to obtain reliable estimates of the parameters. The approach uses multiple sets of broadband rotated coordinates to systematically decouple the parameters in such a way that the most sensitive parameters are found first. Initial tests of the method, using simulated data, are presented in this paper.

Matched-field processing (MFP) is widely used for source localization. Historically, MFP was first performed using complex spectra at a single frequency recorded on a vertical line array (VLA). To overcome ambiguities inherent to single-frequency MFP, broadband MFP was introduced. For a review of the literature about MFP, the reader is referred to Refs. 1 and 2, and the references provided therein. One problem facing MFP efforts is environmental mismatch: the use in MFP of replica vectors that are computed from inaccurate environmental information.<sup>3</sup>

To obtain better environmental information, a variety of matched-field inversion methods, often referred to as environmental or geoacoustic inversion methods, have been developed. Examples of environmental inversion methods are provided in Refs. 4–21 and the references therein. The general goal of environmental inversion methods is to find the properties of the ocean environment that minimize a matched-field cost function or, equivalently, that maximize the correlation between acoustic data and corresponding modeled values. In real cases, environmental inversion results are often hampered by inaccurate information about the source location.

The inversion algorithms most commonly used for environmental inversion can be divided into three categories: local, global, and hybrid methods. Local inversion methods use

the gradients of the cost function and tend to find the minimum closest to the starting position. Global inversion methods, such as simulated annealing<sup>6–8</sup> and genetic algorithms,<sup>9</sup> are based on random jumps that cover more of the cost function search space and thus are more likely to find the global minimum instead of becoming trapped in a local minimum. Hybrid models combine a gradient method with a global method to increase efficiency.<sup>10–13</sup>

In the underwater environment, there is often a correlation between how various parameters influence acoustic propagation. While genetic algorithms are not strongly affected<sup>14</sup> by these parameter correlations or couplings, simulated annealing inversions, in which the physical parameters are varied directly to search for the minimum, are affected. The problems caused by parameter couplings in simulated annealing can be overcome by adding a gradient component to the global search. Hybrid inversions, such as those described in Refs. 10–13, represent ways in which this may be done. Another option is to employ a rotated coordinate system to navigate the parameter search space. The rotated coordinates, which are based on gradient information, are better aligned with the primary features of the search space than are the standard physical parameters.

The method of rotated coordinates was introduced in Ref. 15 and has been used in simulated annealing to obtain environmental parameters accurately and efficiently. The rotated coordinates correspond to the orthogonal transformation that diagonalize the covariance matrix of the cost function gradient. In Refs. 15–17, inversions are performed using rotated coordinates calculated from single-frequency data. Because the individual frequencies are sensitive to different parameters, each single-frequency inversion yields accurate estimates for the parameters that are most sensitive at that frequency. In Ref. 15, the single-frequency results are combined to yield reliable estimates for more of the environmental parameters. In Ref. 18, rotated coordinates calculated for

broadband data are used in geoacoustic inversion. A similar reparametrization based on diagonalizing the model covariance matrix is employed in Ref. 19, in sampling at the critical temperature, and in Refs. 20 and 21, in a Bayesian inversion technique based on a fast Gibbs sampler algorithm to obtain both source and environmental parameters.

The method presented here builds on previous work and expands the possibility for efficiently obtaining reliable parameter estimates. The current work is based on a coherent broadband cost function, introduced in Ref. 2, in which correlations between modeled and measured cross spectra are summed coherently over multiple frequencies. This fully coherent cost function has been applied to broadband matched-field processing analysis.<sup>2,22</sup> The rotated coordinates obtained from the coherent broadband cost function describe the relative sensitivities of the broadband acoustic field to changes in the parameters and the couplings between the parameters.

In the current work, both the source location and the shallow water environment are assumed to be unknown. The three parameters that define the source location are depth, range, and bearing to the horizontal line array (HLA). By allowing both the source and environmental parameters to vary in the inversion, there is the potential to overcome the difficulties of both environmental mismatch in MFP and inaccurate source information in environmental inversion. Examples of previous inversions for both source and environmental parameters include Refs. 20 and 23. Rotated coordinates calculated for both source and environmental parameters provide insights into the parameter couplings and relative sensitivities of the cost function to changes in the parameters over the specified bounds. The rotated coordinates confirm the general parameter hierarchy accepted by the underwater acoustics community:<sup>23</sup> the cost function is much more sensitive to changes in the source parameters than to changes in the environmental parameters when large bounds are allowed on all the parameters.

The wide range of sensitivities of the cost function to changes in the various parameters makes it extremely difficult to obtain reliable estimates of a large number of parameters from a single inversion. The details underlying this difficulty are explained in Sec. III. A method called systematic decoupling using rotated coordinates (SDRC) has been developed to address this problem. In the SDRC approach, multiple sets of broadband rotated coordinates, corresponding to subsequently smaller parameter bounds, are used in a series of inversions to obtain the desired parameter estimates. As shown in this paper, the SDRC method can obtain reliable estimates for the sensitive parameters very efficiently and robustly. The SDRC inversion algorithm is a generalized, iterative inversion technique that can be employed with any cost function, parameter set, or forward model.

The remainder of the paper is organized as follows. In Sec. II, the method of rotated coordinates is presented. The systematic decoupling approach is explained in Sec. III. The performance of the SDRC method to invert for source and environmental parameters is then evaluated using simulated data. Conclusions and current work are discussed in Sec. IV.

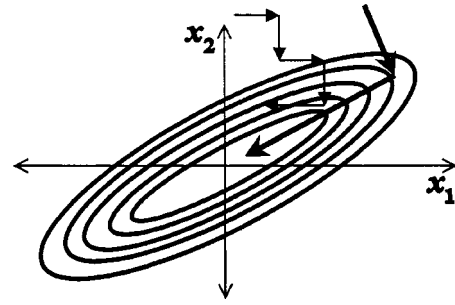


FIG. 1. Contours of a two-dimensional cost function that depict how the parameters  $x_1$  and  $x_2$  are coupled. The thin arrows illustrate the steps taken by an inversion method when the physical parameters are varied. The bold arrows indicate the directions of the steps when rotated coordinates are employed.

## II. ROTATED COORDINATES

The basic concept of rotated coordinates is to use information about the coupling of the parameters to more efficiently navigate the search space in an inversion algorithm.<sup>15</sup> In general, rotated coordinates define directions approximately parallel and perpendicular to the prominent valleys of the cost function search space and thus are an efficient parametrization for the inversion. Figure 1 illustrates possible contours of a two-dimensional cost function. In this example, parameters  $x_1$  and  $x_2$  are coupled, and the resulting valley in the search space is oriented obliquely to the standard parameter axes. In a traditional inversion method, the standard coordinates  $x_1$  and  $x_2$  are varied as illustrated by the thin arrows in Fig. 1. In contrast, the bold arrows in Fig. 1 indicate a parametrization for navigating the search space when rotated coordinates are used. Rotated coordinates increase both the efficiency and the robustness of an inversion.

The rotated coordinates correspond to the orthogonal transformation that diagonalizes the covariance matrix of the cost function gradient  $\mathbf{K}$ . The rotated coordinates are calculated by performing an eigenvalue decomposition (EVD) of  $\mathbf{K}$ , where the elements of  $\mathbf{K}$  are defined as

$$K_{ij} = \int_{\Omega} \frac{\partial E}{\partial x_i} \frac{\partial E}{\partial x_j} d\Omega. \quad (1)$$

A dimensionless parameter array  $\mathbf{x}$  is used so it is meaningful to compare the partial derivatives of the cost function  $E$  with respect to the individual elements of  $\mathbf{x}$ . The dimensionless parameters  $\mathbf{x}$  are obtained by dividing each physical parameter  $a_i$  by  $(a_{\max,i} - a_{\min,i})$ , where  $\mathbf{a}_{\max}$  and  $\mathbf{a}_{\min}$  contain the minimum and maximum values of the physical parameters.  $\Omega$  contains the dimensionless bounds on the integration:  $\{\mathbf{x}_{\max}, \mathbf{x}_{\min}\}$ . An efficient Monte Carlo integration scheme is used to approximate the integral.<sup>15,24</sup> At each point in the Monte Carlo integration, numerical partial derivatives are evaluated:

$$\frac{\partial E}{\partial x_i} = \frac{E(x_i + \Delta x_i) - E(x_i - \Delta x_i)}{2\Delta x_i}, \quad (2)$$

where  $\Delta x_i$  is chosen such that Eq. (2) gives good local derivatives.

An EVD of  $\mathbf{K}$  yields its eigenvectors  $\{\mathbf{v}_j\}$  and the eigenvalues  $\{s_j\}$ . The eigenvectors  $\{\mathbf{v}_j\}$  are referred to as the ro-

TABLE I. Case 1 based on the Workshop97 WA case. The values used to generate the simulated data set for case 1 and the bounds on the nine parameters that define the parameter search space and the bounds for the integration,  $\Omega$  in Eq. (1). The variables are defined in the text.

Parameters	True	Min.	Max.
$z_s$ -m	26.42	10	30
$r_0$ -km	2.22	2.00	2.40
$h_w$ -m	115.3	110	120
$h_1$ -m	27.1	10	50
$\rho_1$ -g/cm <sup>3</sup>	1.54	1.4	1.85
$c_1$ -m/s	1516	1500	1600
$c_{1\text{bot}}$ -m/s	1573	1550	1750
$\rho_2$ -g/cm <sup>3</sup>	1.85	1.60	2.0
$c_2$ -m/s	1751	1600	1800

tated coordinates and provide information about the parameter coupling. The eigenvalues  $\{s_i\}$  identify the relative sensitivities of the cost function  $E$  to changes in the corresponding eigenvectors. Thus, the eigenvectors associated with the largest eigenvalues correspond to the combination of standard parameters that, when varied over the bounds  $\Omega$ , affect the cost function the most. The coupling and the relative sensitivities of the parameters, reflected in the eigenvectors and eigenvalues of  $\mathbf{K}$ , depend on the bounds of the multidimensional integration  $\Omega$ . When large bounds are allowed for a parameter, the parameter is more likely to be represented in an eigenvector associated with a larger eigenvalue than when smaller bounds are used.

The bounds  $\Omega$  are selected on the basis of the specific case being studied and can reflect the uncertainty of the initial values. In the first set of examples (case 1), the bounds specified for the nine unknowns in Table I are used to calculate the rotated coordinates. The latter examples (case 2) use larger parameter bounds on 15 parameters, defined in Table II, similar to bounds that might be used when little is known about the source or the environment. The large bounds in Table II cover a wide range of source positions and the majority of physical values for the ocean sediments.<sup>25</sup> In both cases, no external constraints are used to match physical sedi-

TABLE II. Case 2: The correct environmental values for the case 2 simulated data set and the bounds on the 15 parameters that define the parameter search space and the bounds for the integration,  $\Omega$  in Eq. (1). The variables are defined in the text in Sec. II C.

Parameters	True	Min.	Max.
$z_s$ -m	40	1	70
$r_0$ -km	2.218	0.1	10.0
$\theta$ -deg.	-18.2	-90	90
$h_1$ -m	25	2	50
$\rho_1$ -g/cm <sup>3</sup>	1.37	1.0	3.0
$c_1$ -m/s	1510	1490	1800
$\alpha_{11}$ -dB/m/kHz	0.005	0.0	0.5
$g c_1$ -1/s	1.0	0.0	5.0
$\alpha_{12}$ -dB/m/kHz	0.008	0.0	0.5
$h_2$ -m	50	2	80
$\rho_2$ -g/cm <sup>3</sup>	2.0	1.0	3.0
$r c_2 = c_2 / c_{1\text{bot}}$	1.14	0.9	1.3
$\alpha_{21}$ -dB/m/kHz	0.06	0.0	0.5
$g c_2$ -1/s	0.2	0.0	5.0
$\alpha_{22}$ -dB/m/kHz	0.12	0.0	0.5

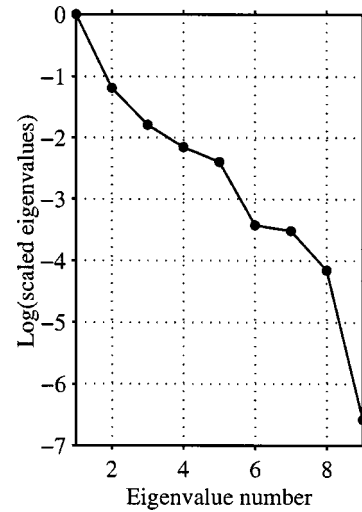


FIG. 2. Example of eigenvalues for case 1 data described in Sec. II C, calculated using the bounds defined in Table I and 720 points in the Monte Carlo integration. The eigenvalues are scaled by the largest eigenvalue; the log of the resulting scaled eigenvalues is shown.

ment properties (to match high sound speeds with high densities, for example).

An example of the eigenvalues and the eigenvectors of  $\mathbf{K}$  is given in Figs. 2 and 3. The cost function  $E$  is defined in Eq. (3), and details of the simulated data set (case 1) are given in Sec. II C. The parameter array  $\mathbf{x}$ , includes nine values that describe the source location, the water depth  $h_w$ , a sediment layer, and a half-space. The two source parameters are  $z_s$  and  $r_0$ , which correspond to the source depth and the range from the source to the horizontal line array (HLA). The four unknown parameters for the sediment layer are thickness  $h_1$ , density  $\rho_1$ , and compressional sound speed at the top and bottom of the layer  $c_1$  and  $c_{1\text{bot}}$ . The two unknowns in the half-space are density  $\rho_2$  and compressional sound speed  $c_2$ . The bounds  $\Omega$  for the Monte Carlo integration of Eq. (1) are shown in Table I. The resulting scaled

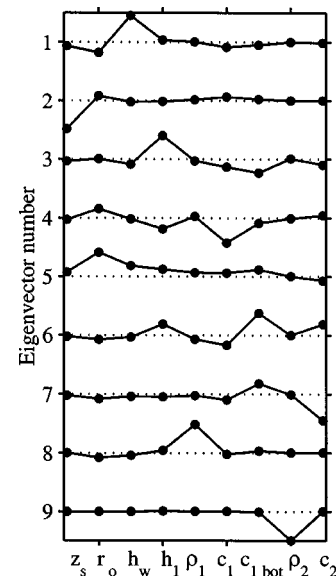


FIG. 3. Example of eigenvectors corresponding to the eigenvalues in Fig. 2. Parameters that have large amplitudes in an eigenvector are coupled.

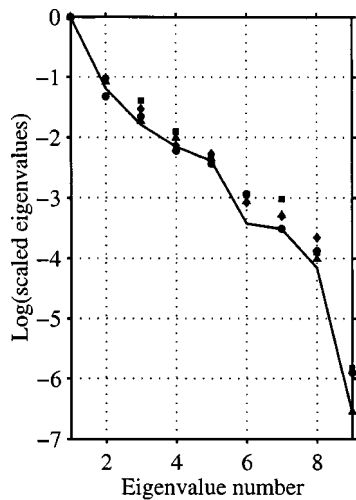


FIG. 4. Comparison of scaled eigenvalues, similar to Fig. 2, obtained when 30 (circles), 60 (diamonds), 120 (squares), 360 (triangles), 720 (line) Monte Carlo samples are used to approximate the integral in Eq. (1).

eigenvalues and eigenvectors are shown in Figs. 2 and 3, respectively.

The eigenvectors in Fig. 3 or, equivalently, the rotated coordinates indicate which standard parameters are coupled in this example. In the first eigenvector, the elements corresponding to  $h_w$ ,  $r_0$ , and  $c_1$  have the largest values, indicating they are coupled: changes in  $h_w$  will most likely decrease the cost function if the corresponding changes are also made in  $r_0$  and  $c_1$  as shown in the first eigenvector. Likewise, in the second eigenvector,  $z_s$ ,  $r_0$  and  $c_1$  are coupled, indicating the second most likely way to decrease the cost function. The third eigenvector indicates a coupling between  $h_1$ ,  $h_w$ ,  $c_1$ ,  $c_{1\text{bot}}$ , and  $c_2$ , and so forth.

The eigenvalues indicate the relative sensitivity of the cost function to changes in the eigenvectors over the specified parameter bounds. In Fig. 2, the eigenvalues have been scaled by the largest one, and the log of the resulting scaled eigenvalues is plotted. The eigenvalue associated with the first eigenvector is significantly larger than the remaining eigenvalues. Therefore, the parameters that have the most influence on the cost function, when allowed to vary over the bounds in Table I, are represented in the first eigenvector.

One question about the calculation of the rotated coordinates concerns the convergence of the Monte Carlo approximation to the integral in Eq. (1). To address how the number of Monte Carlo points affects the rotated coordinates, Figs. 4 and 5 show the scaled eigenvalues and rotated coordinates when 30 (circles), 60 (diamonds), 120 (squares), and 360 (triangles) Monte Carlo samples are included in the approximation of the integral. The solid lines indicates the values when 720 samples are used, as shown in Figs. 2 and 3. The different sets of scaled eigenvalues in Fig. 4 are comparable, and the parameters represented in the first several eigenvectors in the various cases in Fig. 5 are the same, with the occasional exception of a negative sign. When the bounds on the parameters are larger, the agreement between the sets of rotated coordinates often degrades slightly with increasing parameter number. For the iterative algorithm presented in this paper, however, only the structure of the first few rotated

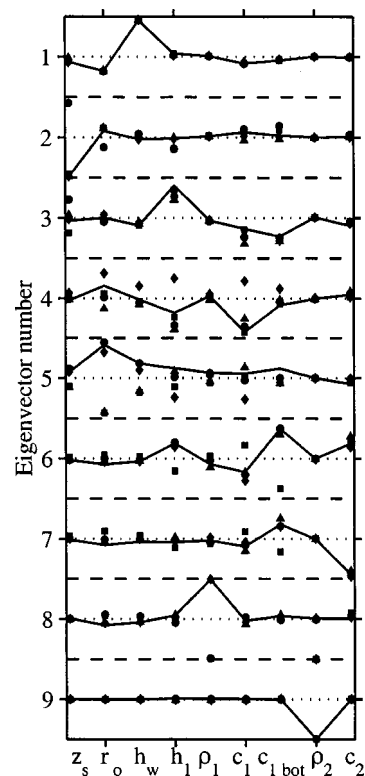


FIG. 5. Comparison of rotated coordinates, similar to Fig. 3, obtained when 30 (circles), 60 (diamonds), 120 (squares), 360 (triangles), and 720 (lines) Monte Carlo points are used, as in Fig. 4. The horizontal dashed lines separate the eigenvectors.

coordinates is important because only the rotated coordinates with relatively large eigenvalues are used in the inversion.

### A. Cost function

The rotated coordinates technique can be used with any cost function. In our method, a coherent broadband cost function is employed so that the broadband features of the search space are reflected in the rotated coordinates. The cost function used in our analysis was first introduced in Ref. 2 and is defined as

$$E(\mathbf{x}) = 1 - C(\mathbf{x}), \quad (3)$$

where  $C(\mathbf{x})$  is the coherent broadband correlation between data and model cross spectra for the set of source and environmental parameters  $\mathbf{x}$ :

$$C(\mathbf{x}) = \sum_f \sum_j \sum_{i>j} D_i(f) D_j^*(f) M_i^*(f, \mathbf{x}) M_j(f, \mathbf{x}), \quad (4)$$

where  $i$  and  $j$  indicate the receivers, and  $f$  denotes frequency.  $D_i(f)$  is the measured spectra on the  $i$ th hydrophone at frequency  $f$  and is normalized such that

$$\sqrt{\sum_f \sum_j \sum_{i>j} |D_i(f) D_j^*(f)|^2} = 1. \quad (5)$$

The source and environmental parameters in  $\mathbf{x}$  are used to calculate the modeled spectral values  $M_i(f, \mathbf{x})$  for the  $i$ th hydrophone at frequency  $f$ , which are normalized in the same manner:

$$\sqrt{\sum_f \sum_j \sum_{i>j} |M_i(f, \mathbf{x}) M_j^*(f, \mathbf{x})|^2} = 1. \quad (6)$$

It is important to note that the diagonal elements in Eq. (4) are not included in the coherent sum. There are two reasons for the exclusion of the diagonal terms. First, the exclusion reduces the severity of the side lobes in the ambiguity patterns. Second, the exclusion increases the coherence gain of the signal relative to assumed incoherent noise.<sup>2</sup>

## B. Simulated annealing

The rotated coordinates are used to construct the explicit expression for the parameter perturbations in the simulated annealing optimization. Specifically, at each step in the inversion, a single eigenvector  $j$  is perturbed, and the new values of the standard dimensionless coordinates  $\mathbf{x}'$  are

$$\mathbf{x}' = \mathbf{x} + \frac{1}{2} \gamma^3 \mathbf{v}_j, \quad (7)$$

where  $\gamma$  is randomly selected from the interval  $(-1, 1)$ . The cubed power of the random number  $\gamma$  in Eq. (7) allows large perturbations, but tends towards small perturbations, as described in Ref. 15, and is efficient with the linear cooling schedule used in the fast simulated annealing algorithm.<sup>8</sup> In the inversion, each eigenvector is used one time to vary the parameters, as shown in Eq. (7), before the temperature is reduced. From Eq. (7), it is clear that a single rotated coordinate can vary all the physical parameters.

## C. Numerical results for traditional and rotated coordinates annealing

To evaluate the ability of the rotated coordinates inversion method to find source and environmental parameters, two simulated data sets are used. The first data set considered is based on the WA case from the 1997 Geoacoustic Inversion Workshop<sup>4</sup> (Workshop97) and consists of broadband signals received on an evenly-spaced HLA. The nine unknowns correspond to source position, water depth, single sediment layer and half-space properties. In the second case, a realistic tapered HLA is used, and the environment is described by two sediment layers over a half-space. In case 2,

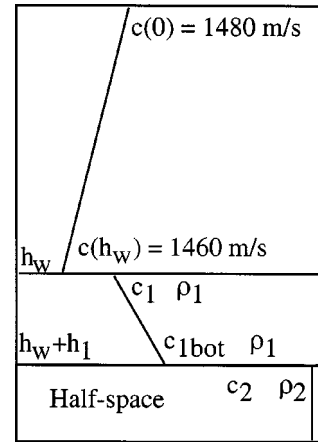


FIG. 6. Environment for the simulated data for case 1. The values of the environmental parameters are listed in Table I.

larger bounds are allowed on the source location and environmental parameters. The range-independent normal mode model ORCA<sup>26</sup> is used to generate the synthetic broadband data. The data  $D_i(f)$  and the modeled values  $M_i(f)$ , which are computed by ORCA for the examples presented in this paper, are compared using the cost function in Eq. (3). For the following examples, 40 frequencies, evenly spaced between 50 and 250 Hz, are included in the sum over frequencies.

### 1. Case 1

Simulated data for case 1 is based on the WA case from Workshop97, which is illustrated in Fig. 6. The nine unknowns are source depth and range,  $z_s$  and  $r_0$ , water depth  $h_w$ , four sediment parameters, thickness  $h_1$ , density  $\rho_1$ , and compressional sound speed at the top and bottom of the layer  $c_1$  and  $c_{1bot}$ , and two half-space parameters, density  $\rho_2$  and compressional sound speed  $c_2$ . The parameter values used to generate the data and the bounds on the search space are given in Table I. The synthetic data set consists of broadband complex spectra values received on a 51-element, evenly spaced HLA with total horizontal aperture of 500 m at a depth of 75 m. The resulting scaled eigenvalues and rotated

TABLE III. Comparison of solutions obtained by a simulated annealing inversion algorithm when standard coordinates (third column) and the various sets of rotated coordinates in Fig. 5 are varied. The bounds in Table I are used to calculate the rotated coordinates and to define the inversion search space  $\Omega$ . The total number of forward calls to the model, on the last line, includes the calculation of the rotated coordinates. The correct values are shown in Table I.

	Initial values	phys. coords.	720 pts.	360 pts.	120 pts.	60 pts.	30 pts.
$z_s$ -m	20	26.3	26.6	26.7	26.4	26.4	26.5
$r_0$ -km	2.00	2.213	2.221	2.231	2.203	2.217	2.207
$h_w$ -m	100	115.2	115.6	115.5	114.9	115.3	115.0
$h_1$ -m	50	25.5	26.4	26.1	26.6	26.7	25.1
$\rho_1$ -g/cm <sup>3</sup>	1.5	1.58	1.61	1.64	1.59	1.64	1.71
$c_1$ -m/s	1550	1524	1518	1516	1517	1519	1520
$c_{1bot}$ -m/s	1700	1558	1572	1572	1567	1568	1558
$\rho_2$ -g/cm <sup>3</sup>	2.0	1.76	1.63	1.98	1.63	1.78	1.94
$c_2$ -m/s	1800	1708	1711	1703	1723	1723	1701
$E$	0.768	0.007	0.009	0.008	0.006	0.006	0.009
Calls		80 000	31 500	24 300	22 300	19 200	18 750

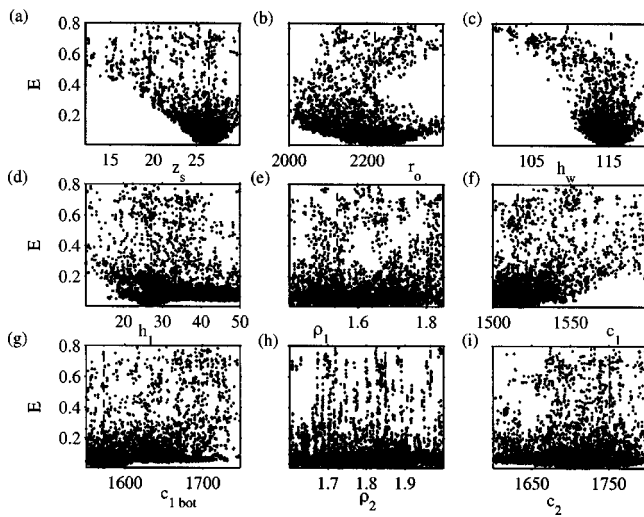


FIG. 7. Scatter plots of the cost function versus the individual parameters for all the states visited in the inversion detailed in Table III.

coordinates obtained using various number of points to approximate the integral in Eq. (1) are shown in Figs. 2–5.

Table III shows the results of inversions when the physical and the rotated coordinates are varied. The initial parameter values are given in the second column. The third column contains the inversion results from classical simulated annealing using the physical parameters. The remaining columns show the inversion results when the various sets of rotated coordinates shown in Fig. 5 are used in fast simulated annealing as described previously. Similar cost function values and parameter estimates are found in all cases. The rotated coordinates' inversions are, however, more efficient.

The variations in the parameter estimates result from the non-uniqueness of the inverse problems using the cost function and the input data. To illustrate this uncertainty, plots of the cost function  $E$  as a function of the individual parameters at all states visited in the inversion are considered in Fig. 7.

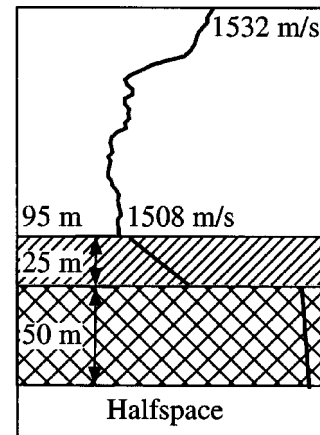


FIG. 8. Environmental model for case 2 simulated data.

The width of the distributions for low values of  $E$  indicate both the sensitivity, or lack of sensitivity, to changes in the parameters and provide estimates of the uncertainty in the inversion results.

## 2. Case 2

As the number of unknowns in the inversion increases, both the traditional annealing method and the rotated coordinates method have more difficulty finding good parameter estimates. To illustrate these difficulties, a simulated data set, referred to as case 2, is used. The source location and the properties of the shallow ocean environment in this example are given in the second column of Table II. The realistic downward refracting sound speed profile is shown in Fig. 8. The water depth is 95 m. The 52 receivers are located on a tapered, bottom-mounted array that covers a horizontal aperture of 568 m.

In case 2 there are 15 unknown parameters. The three source parameters that identify the source location are  $z_s$ ,  $r_0$ , and  $\theta$ , which correspond to the source depth, the range,

TABLE IV. Inversion results of case 2 data for the parameters that define the source location and the two sediment layers when standard coordinates (fourth column) and rotated coordinates (fifth column) are varied. The bounds on the parameters for both the rotated coordinates calculation and the inversion are found in Table II. The parameter numbers in the first column are used for identification in Figs. 10 and 11.

No.	Parameter	Initial values	Results: standard	Results: rotated	Correct values
1	$z_s$ -m	6	19.1	39.5	40
2	$r_0$ -km	5.0	2.224	2.228	2.218
3	$\theta$ -deg	90	-18.2	-18.2	-18.2
4	$h_1$ -m	40	32.3	25.2	25
5	$\rho_1$ -g/cm <sup>3</sup>	1.80	1.70	1.51	1.37
6	$c_1$ -m/s	1700	1521	1504	1510
7	$\alpha_{11}$ -dB/m/kHz	0.05	0.033	0.015	0.005
8	$g c_1$ -1/s	0.05	0.004	1.47	1.0
9	$\alpha_{12}$ -dB/m/kHz	0.05	0.41	.013	0.008
10	$h_2$ -m	20	80	39.8	50
11	$\rho_2$ -g/cm <sup>3</sup>	1.6	1.05	2.3	2.0
12	$r c_2 = c_2 / c_{1bot}$	0.912	1.17	1.114	1.14
13	$\alpha_{21}$ -dB/m/kHz	0.01	0.002	0.228	0.06
14	$g c_2$ -1/s	0.005	0.02	2.95	0.2
15	$\alpha_{22}$ -dB/m/kHz	0.01	0.17	0.49	0.12
	$E$	0.995	0.161	0.073	0.005
	Forward calls		80,000	29,000	

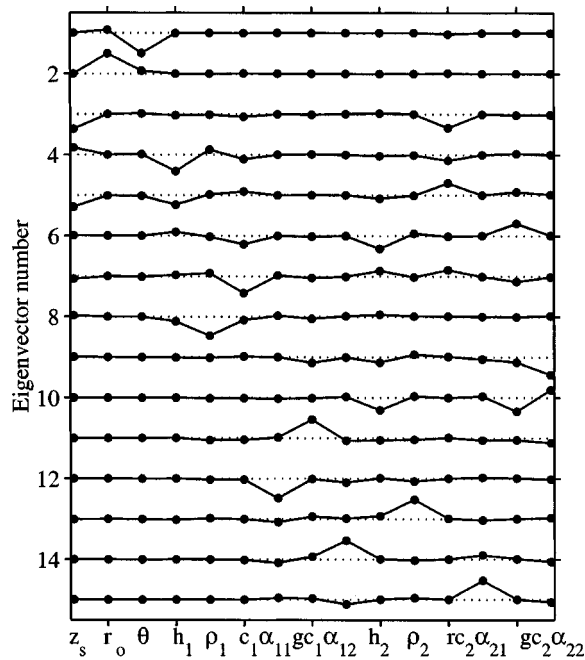


FIG. 9. Rotated coordinates for case 2 data employed in inversion shown in Table IV.

and the bearing from the source to the horizontal line array (HLA). Each of the two sediment layers  $i=1,2$  is characterized by six parameters: thickness  $h_i$ , density  $\rho_i$ , compressional sound speed at the top of the layer  $c_i$ , or ratio of the compressional sound speeds at the interface  $rc_i = c_i/c_{i-1\text{bot}}$ , gradient of the compressional sound speed in the layer  $gc_i$ , and compressional attenuations at the top and bottom of the layer,  $\alpha_{i1}$  and  $\alpha_{i2}$ . The half-space parameters are held fixed.

Table IV shows the results when both standard annealing with physical parameters and fast annealing with rotated coordinates are used to find the 15 parameters that define the source location and the two sediment layers using the case 2 data. The rotated coordinates used in this example, shown in Fig. 9, are calculated using 120 points to evaluate the integral in Eq. (1) over the bounds given in Table II. Figures 10 and 11 show the progression of the standard and the rotated coordinates inversions. Both methods obtain good estimates for the most sensitive parameters,  $r_0$ ,  $\theta$ ,  $c_1$ , and  $rc_2$ . The rotated coordinates method also yields reasonably close values for two other parameters,  $z_s$  and  $h_1$ , and, in addition, takes less time than the standard annealing method.

In summary, the inversion method presented here uses coherent broadband rotated coordinates related to the parameter couplings to navigate the parameter search space and to find the parameters  $\mathbf{x}$  that minimize the cost function in Eq. (3). The efficiency of the inversion is improved when rotated coordinates are used.

### III. SYSTEMATIC DECOUPLING

The ability of the rotated coordinates method to find good estimates for a large number of parameters in a single inversion is not guaranteed. To improve the robustness of the rotated coordinates inversions, the method of systematic de-

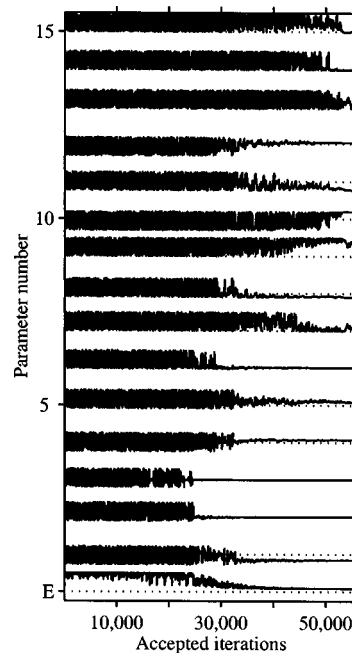


FIG. 10. The accepted values in the inversion using standard coordinates for the cost function  $E$  and the 15 parameters detailed in Table III. The horizontal lines indicate the correct parameter values.

coupling using rotated coordinates (SDRC) has been developed. In this section, traditional techniques used to improve annealing results are discussed. Motivation for use of the SDRC method is provided, and the SDRC method is described. Examples are given to illustrate how the SDRC method improves the likelihood and the efficiency of obtaining reliable estimates for the sensitive parameters.

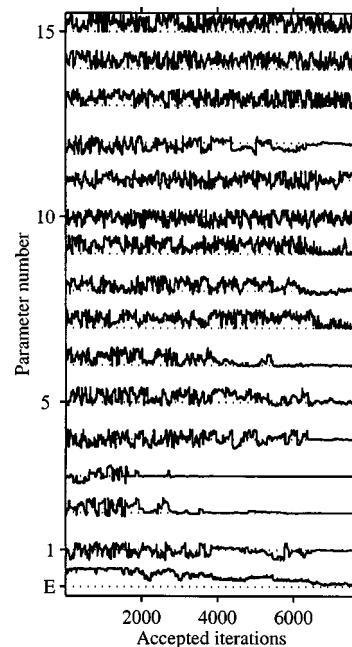


FIG. 11. The accepted values in the inversion using the rotated coordinates in Fig. 9 for the cost function  $E$  and the 15 parameters detailed in Table III. The horizontal lines indicate the correct parameter values.

TABLE V. Example of SDRC method to obtain estimates for three source parameters and three sediment parameters. The numbers in the first column correspond to the parameter numbers in Figs. 12 and 13.

No.	Parameter	Initial	Step 1	Step 2	Step 3	Step 4	Step 5	Correct
1	$z_s$ -m	6	5.4	23	36.9	40.3	40.9	40
2	$r_0$ -km	5.0	4.279	2.196	2.042	2.170	2.218	2.218
3	$\theta$ -deg	90	-20.0	-18.4	-18.3	-17.8	-18.2	-18.2
4	$h_1$ -m	5.0	11.2	41.9	49.8	23.2	25.2	25
5	$c_1$ -m/s	1600	1587	1518	1495	1506	1510	1510
6	$gc_1$ -1/s	0.0025	4.77	3.37	4.33	0.58	1.07	1.0
	$E$	0.997	0.85	0.40	0.33	0.14	0.032	0.005
	$n_{var}$		2	4	5	6	6	

### A. How to obtain good estimates with simulated annealing

Several methods have been developed to improve the results of simulated annealing. Some of these techniques are to adjust the initial temperature, the cooling schedule (in traditional annealing), and the convergence criteria. Additional methods often used to obtain better inversion results include trying multiple initial values and reducing the bounds on the parameter search space. Another scheme is to divide the parameters into two or more groups and to initially vary only the parameters in the first group while holding the rest fixed. Then, the parameters in the second group are varied while the others are held at the values obtained by the first inversion. The pattern is repeated. An example of this grouping method is found in Ref. 27. While the basic idea of decoupling the parameter set is useful, some unsatisfactory aspects of this grouping method are that (1) the user must decide how to group the parameters, and (2) there is the possibility that holding sensitive parameters at initial or intermediate incorrect values badly influences the results.

While these different refining techniques result in better annealing estimates, they are most useful when the user knows *a priori* the values he wants to obtain. In the case of experimental or other real data, one rarely has the luxury of knowing the correct answers. A primary goal in the present work is to improve the robustness of simulated annealing by developing an algorithm that works well when little is known about the correct values of the parameters and that depends less on the specific values chosen for the annealing temperature, the convergence criteria, the initial parameter values, and the parameter bounds.

### B. Motivation

The underlying problem that hampers inversion efforts for a large number of unknown parameters is that less sensitive parameters cannot be reliably obtained if the value of the cost function is large because of errors in the more sensitive parameters. At relatively large values of the cost function, there are a wide range of values for the less sensitive parameters that give the same cost function value. The cost function must be reduced by finding good estimates for the most sensitive parameters before estimates of the less sensitive parameters can be found. Thus, the basic idea underlying the SDRC algorithm is to find estimates for the most sensitive parameters first, to reduce the bounds on those parameters in  $\Omega$ , and then to find estimates for the less sensitive parameters. SDRC is accomplished by a series of inversions using multiple sets of rotated coordinates, each set corresponding to subsequently smaller sets of parameter bounds on the integration  $\Omega_i$ . Each inversion is referred to as a step.

While the SDRC method is reminiscent of the grouping method discussed at the end of the previous section, the important difference is that the user does not make the decisions. The number of rotated coordinates used to vary the parameters during each inversion is determined by the properties of the cost function, which are based on the data. Specifically, for each set of rotated coordinates, the eigenvalues are used to decide which rotated coordinates to vary in that inversion. The rotated coordinates used in the inversion are termed the primary rotated coordinates. The primary rotated coordinates are defined as those with scaled eigenvalues within  $\beta$  of the largest eigenvalue, where  $\beta$  is typically chosen to be 40 or 60 dB to include eigenvalues within two or

TABLE VI. Bounds  $\Omega_i$  on the six parameters for the rotated coordinates calculation in the last four steps of the SDRC inversion given in Table V. The bounds on the rotated coordinates calculation in step 1  $\Omega_1$  are listed in Table II. The bounds in Table II define the limits on the annealing search space for all five steps.

Parameter	Step 2		Step 3		Step 4		Step 5	
	min	max	min	max	min	max	min	max
$z_s$ -m	1	70	1	70	20	60	30	50
$r_0$ -km	1.5	6.5	1.7	2.7	1.7	2.3	2.0	2.3
$\theta$ -deg	-23	-16	-23	-16	-23	-16	-19	-17
$h_1$ -m	2	50	2	50	2	50	2	50
$c_1$ -m/s	1495	1800	1495	1800	1495	1800	1495	1600
$gc_1$ -1/s	0	5	0	5	0	5	0	5

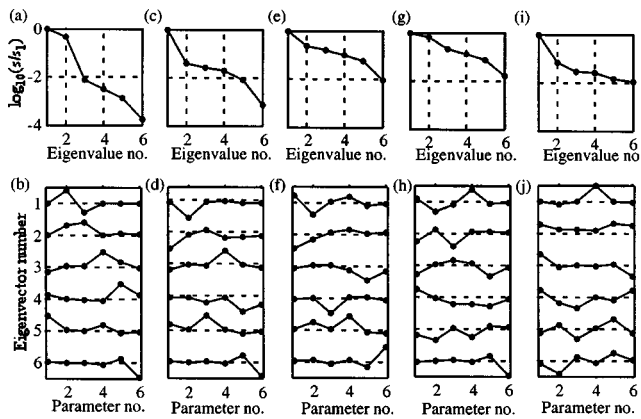


FIG. 12. Eigenvalues and eigenvectors for the SDRC inversion detailed in Table V: step 1 in (a) and (b), step 2 in (c) and (d), step 3 in (e) and (f), step 4 in (g) and (h), step 5 in (i) and (j).

three orders of magnitude of the largest one. While only a subset of the rotated coordinates are employed in the inversion, each rotated coordinate can potentially change all the physical parameter values.

The physical parameters represented in the primary rotated coordinates change as the bounds on the integration  $\Omega$  are adjusted. As the bounds on a parameter decrease, the likelihood also decreases that the parameter has a significant value in a primary rotated coordinate. In the SDRC method, each step corresponds to a new set of parameter bounds  $\Omega_i$ , so that the parameters represented in each set of primary rotated coordinates are most likely to differ. Specifically, each parameter is represented in a primary rotated coordinate when the cost function has been reduced to a level at which it is sensitive to changes in that parameter. In this manner, all sensitive parameters can potentially be found regardless of the initial values and the parameter bounds. There are cases where the data is not sensitive to changes in a specific pa-

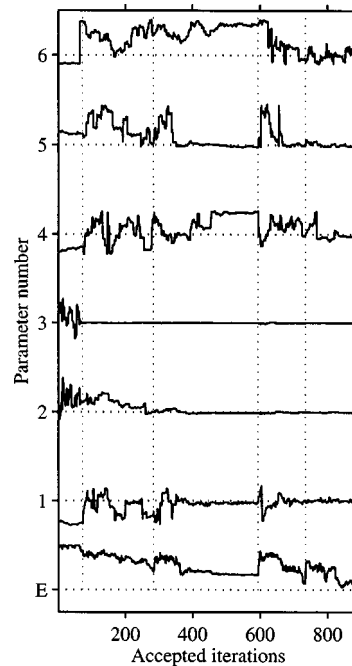


FIG. 13. Accepted parameter states from the five step SDRC inversion detailed in Table V. The horizontal lines indicate the correct parameter values. The vertical lines divide the steps listed in Table V. The cost function increases at the beginning of each step because the initial temperature is reset to a high value.

rameter, independent of the accuracy of the remaining parameter. In such cases, no reliable information about that parameter can be found.

It should be noted here that the success of the SDRC method is independent of the exact number of Monte Carlo points used to approximate the integral in Eq. (1) because the principal features of the primary rotated coordinates are independent of the number of samples, as shown in Fig. 5.

TABLE VII. Results of an SDRC inversion for the 15 parameters that define the source location and the two sediment layers.  $n_{\text{var}}$  is the number of rotated coordinates used in each step to vary the parameters. The numbers in the first column correspond to the parameter numbers in Fig. 14.

No.	Parameter	Initial	Step 1	Step 2	Step 3	Step 4	Step 5	Correct
1	$z_s$ -m	6	7.6	20.5	38.0	39.6	39.6	40
2	$r_0$ -km	5	2.318	2.347	2.187	2.179	2.218	2.218
3	$\theta$ -deg.	90	-19.4	-18.1	-18.2	-18.1	-18.2	-18.2
4	$h_1$ -m	40	39.7	2.3	24.0	24.1	25.0	25
5	$\rho_1$ -g/cm <sup>3</sup>	1.8	1.85	2.43	1.11	1.41	1.39	1.37
6	$c_1$ -m/s	1700	1669	1537	1519	1505	1505	1510
7	$\alpha_{11}$ -dB/m/kHz	0.05	0.048	0.098	0.43	0.036	0.013	0.005
8	$g c_1$ -1/s	0.0025	4.76	4.30	1.32	1.76	1.37	1.0
9	$\alpha_{12}$ -dB/m/kHz	0.05	0.05	0.049	0.18	0.035	0.009	0.008
10	$h_2$ -m	20.0	19.5	41.3	46.5	71.1	50.2	50
9	$\alpha_{12}$ -dB/m/kHz	0.05	0.05	0.049	0.18	0.035	0.009	0.008
10	$h_2$ -m	20.0	19.5	41.3	46.5	71.1	50.2	50
11	$\rho_2$ -g/cm <sup>3</sup>	1.6	1.63	1.45	2.22	2.43	2.31	2.0
12	$r c_2 = c_2 / c_{1\text{bot}}$	0.91	0.92	0.97	1.11	1.14	1.14	1.14
13	$\alpha_{21}$ -dB/m/kHz	0.01	0.10	0.11	0.31	0.05	0.09	0.06
14	$g c_2$ -1/s	0.005	0.067	1.36	1.51	0.72	0.094	0.2
15	$\alpha_{22}$ -dB/m/kHz	0.01	0.032	0.49	0.18	0.49	0.13	0.12
	$E$	0.995	0.64	0.36	0.20	0.083	0.019	0.005
	$n_{\text{var}}$		2	5	9	11	13	

TABLE VIII. Bounds  $\Omega_i$  for the rotated coordinates calculation in the SDRC inversion described in Table VII. The bounds in Table II are used to calculate the rotated coordinates used in the first step and define the annealing search space for all five inversions.

Parameter	Step 2		Step 3		Step 4		Step 5	
	min	max	min	max	min	max	min	max
$z_s$ -m	1	70	1	70	25	50	35	45
$r_0$ -km	0.1	5.0	2.0	2.7	2.1	2.3	2.15	2.25
$\theta$ -deg.	-21	-17	-21	-17	-19	-17.5	-18.7	-17.5
$h_1$ -m	2	50	2	50	2	50	23	26
$\rho_1$ -g/cm <sup>3</sup>	1.0	3.0	1.0	3.0	1.0	3.0	1.0	1.8
$c_1$ -m/s	1490	1800	1490	1800	1490	1800	1495	1530
$\alpha_{11}$ -dB/m/kHz	0.0	0.5	0.0	0.5	0.0	0.5	0.0	0.5
$g c_1$ -1/s	0.0	5.0	0.0	5.0	0.0	5.0	0.0	1.5
$\alpha_{12}$ -dB/m/kHz	0.0	0.5	0.0	0.5	0.0	0.5	0.0	0.5
$h_2$ -m	2	80	2	80	30	80	30	80
$\rho_2$ -g/cm <sup>3</sup>	1.0	3.0	1.0	3.0	1.0	3.0	1.0	3.0
$r c_2 = c_2 / c_{1\text{bot}}$	0.9	1.3	0.9	1.3	1.0	1.3	1.1	1.2
$\alpha_{21}$ -dB/m/kHz	0.0	0.5	0.0	0.5	0.0	0.5	0.0	0.5
$g c_2$ -1/s	0.0	5.0	0.0	5.0	0.0	5.0	0.0	5.0
$\alpha_{22}$ -dB/m/kHz	0.0	0.5	0.0	0.5	0.0	0.5	0.0	0.5

### C. The SDRC algorithm

The SDRC method proceeds as follows. With large bounds on all parameters, the rotated coordinates are calculated. The primary rotated coordinates are used to vary the parameters in simulated annealing. The bounds in  $\Omega_1$  on the most sensitive parameters, those represented in the first one or two rotated coordinates, are reduced. Using the reduced bounds  $\Omega_2$ , a new set of rotated coordinates is calculated. The solution from the first step provides the initial values for the second rotated coordinates annealing, performed using the second set of primary rotated coordinates. The parameter bounds are reduced again to form  $\Omega_3$ , new rotated coordinates are calculated, and another simulated annealing run is performed. This pattern is repeated until all possible parameters are found. It is important to note that while the bounds on the integration for the calculation of the rotated coordinates are being reduced between the steps, the bounds on the annealing search space are never changed. In this manner, the rotated coordinates describe the features of a smaller and smaller region of the search space. The initial large bounds on the annealing search space are maintained to reduce the possibility of confining the search to the vicinity of a local minima.

#### 1. Example of an SDRC inversion for six parameters

An example of an SDRC inversion to obtain estimates for the source location and three sediment parameters is described in Tables V and VI and Figs. 12 and 13. The data for case 2 and 30 Monte Carlo points are used to calculate the rotated coordinates. The third column of Table V gives the initial parameter values and cost function  $E$ . The next five columns give the results of the individual inversions (referred to as steps) performed when the bounds  $\Omega_i$  shown in Table VI are used to calculate the rotated coordinates. The large bounds shown in Table II define the bounds on the annealing search space for all five inversions. The results from step 1 are used as the initial values for step 2, and so

forth. Table V also shows the number of primary rotated coordinates  $n_{\text{var}}$  employed in each step. The initial annealing temperature of each step is  $T_0 = 10$ .

The rotated coordinates and eigenvalues calculated for each set of bounds are shown in Fig. 12. The eigenvalues and rotated coordinates calculated with the large bounds listed in Table II are shown in Figs. 12(a) and (b). Two of the rotated coordinates have scaled eigenvalues within 40 dB of the largest eigenvalue, so they are used to vary the parameters in step 1 of the SDRC inversion. The parameters  $r_0$  and  $\theta$  have the largest components in the first two rotated coordinates; thus, they are primarily varied in the first step. In the second step, where the bounds on  $r_0$  and  $\theta$  have been reduced, four rotated coordinates have eigenvalues within 40 dB of the largest eigenvalue, as shown in Figs. 12(c) and (d), and these

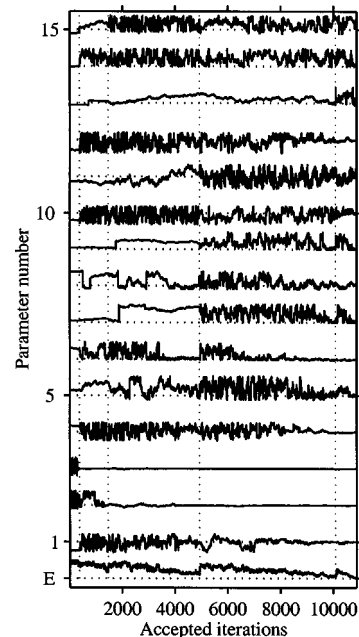


FIG. 14. Progression of the five-step SDRC inversion detailed in Table VII. The vertical lines divide the steps.

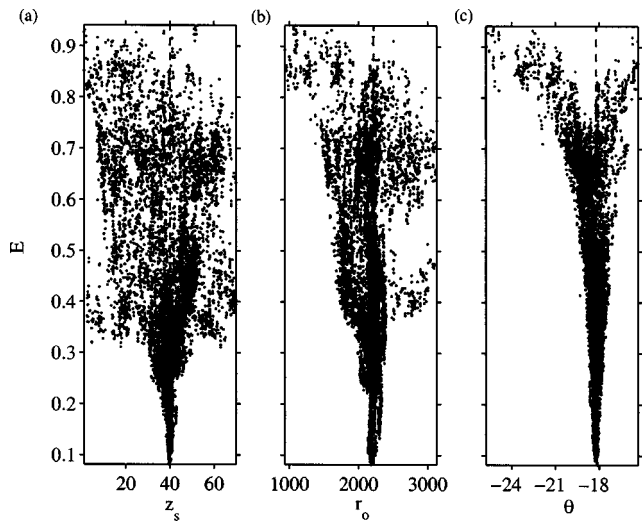


FIG. 15. Scatter plots of the cost function versus (a)  $z_s$ , (b)  $r_0$ , and (c)  $\theta$  for the parameter states sampled in the inversion detailed in Table VII.

four are employed in the annealing. The resulting estimates for  $r_0$  and  $\theta$  are close to the correct answers. Over the reduced parameter bounds  $\Omega_2$ ,  $r_0$  is approximately decoupled from the other parameters because the element corresponding to  $r_0$  is the only large value in the first rotated coordinate. The bounds on  $r_0$  are again reduced. In the third step, Figs. 12(e) and (f), the first five rotated coordinates, which have eigenvalues within 40 dB of the largest eigenvalue are used. The results show a significant improvement in the estimate of  $z_s$ . The bounds on  $r_0$  and  $z_s$  are decreased, and all six of the rotated coordinates calculated for step 4, Figs. 12(g) and (h), have scaled eigenvalues within 40 dB of the largest eigenvalue. The sediment thickness now has the largest value in the first rotated coordinate and is, consequently, the parameter estimate most improved during this step. Bounds are again reduced, and the resulting scaled eigenvalues for step 5 are all within 20 dB of the largest value, as shown in Figs.

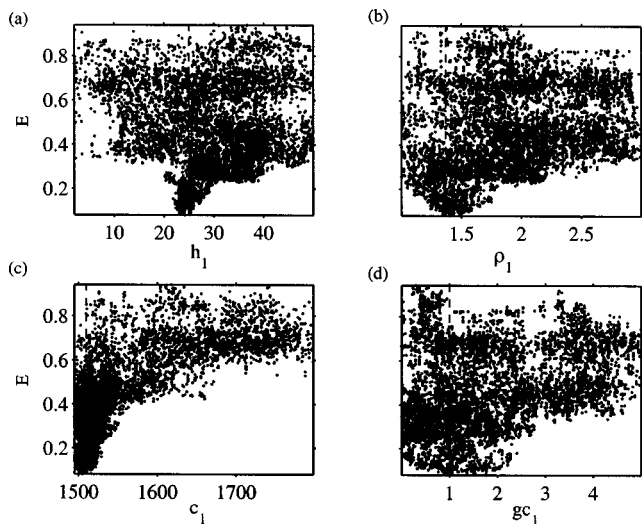


FIG. 16. Scatter plots of the cost function versus the (a)  $h_1$ , (b)  $\rho_1$ , (c)  $c_1$ , and (d)  $gc_1$  for the parameter states sampled in the inversion detailed in Table VII.

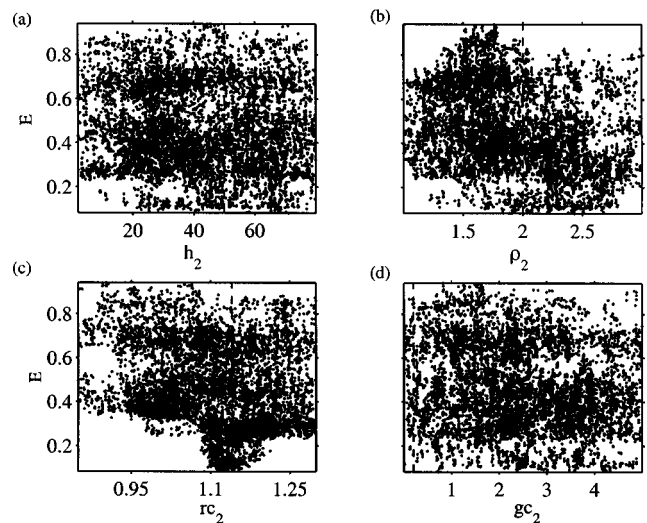


FIG. 17. Scatter plots of the cost function versus the (a)  $h_2$ , (b)  $\rho_2$ , (c)  $rc_2$ , and (d)  $gc_2$  for the parameter states sampled in the inversion detailed in Table VII.

12(i) and (j). Additional steps could be performed to lower the cost function further.

Approximately 7800 forward calls (including the calculations of the rotated coordinates) are made in this five-step process that obtains good estimates for all six parameters. Figure 13 shows the 874 states that are accepted during the five inversions. Accepted iterations 1 to 73 in Fig. 13 correspond to the states accepted during step 1, accepted iterations 74 to 284 represent the progress during step 2, and so forth. The vertical lines in Fig. 13 are placed at the end of each inversion step. During the iterations associated with step 1, when only two rotated coordinates are used, parameters 1, 4, 5, and 6, corresponding to  $z_s$ ,  $h_1$ ,  $c_1$  and  $gc_1$  are not varied significantly. Likewise, parameter 2,  $\theta$ , is not varied significantly after step 1, and parameter 3,  $r_0$ , is not varied much in steps 4–5. The jumps in the cost function at the beginning of each step are caused by resetting the initial temperature to a large value at the beginning of each new inversion.

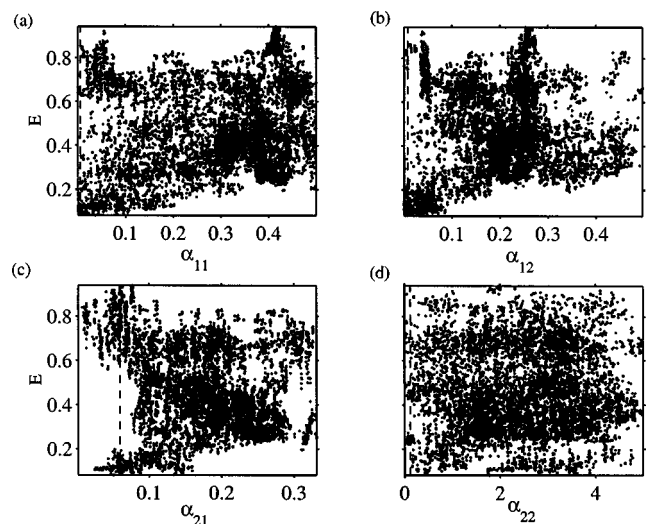


FIG. 18. Scatter plots of the cost function versus the (a)  $\alpha_{11}$ , (b)  $\alpha_{12}$ , (c)  $\alpha_{21}$ , and (d)  $\alpha_{22}$  for the parameter states sampled in the inversion detailed in Table VII.

## 2. Example of an SDRC inversion for 15 parameters

The example of an SDRC inversion for six parameters in the previous section is given to illustrate the SDRC algorithm. The advantages of the SDRC algorithm are more apparent when the number of unknowns in the inversion is larger. The results are now presented for an SDRC inversion for 15 unknown parameters that define the source location and the properties of the two sediment layers for the case 2 data introduced in Sec. II C. Table VII gives the initial parameter values and the results after each of the five inversions, referred to as steps. The bounds used to calculate the rotated coordinates in each step are shown in Table VIII.<sup>28</sup> Thirty Monte Carlo points are used in the calculation of the rotated coordinates. The starting annealing temperature in steps 1–4 is 10 but is reduced to 0.5 for the final step. The number of rotated coordinates employed in each step  $n_{\text{var}}$  is shown at the bottom of Table VII. In steps 1–3, the rotated coordinates with scaled eigenvalues within two orders of magnitude of the largest value are used to vary the parameters. In steps 4 and 5, those with scaled eigenvalues within three orders of magnitude of the largest value are used to allow the least sensitive parameters to be varied in the final steps.

The progression of the SDRC inversion is shown in Fig. 14. The vertical lines separate the inversion steps. The only parameters varied significantly in the first step are  $r_0$  and  $\theta$ . During step 2,  $z_s$ ,  $r_0$ ,  $h_1$ ,  $c_1$ ,  $h_2$ ,  $rc_2$ , and  $gc_2$  have large values in the primary rotated coordinates and are varied. Most of the parameters are varied during steps 3–5. The least sensitive parameter  $\alpha_{21}$  is not varied substantially until the last step.

Approximately 30 000 forward calls were made to complete the SDRC inversion shown in Table VII. The SDRC method not only obtained better estimates for more of the parameters but also made approximately only 1000 more forward calls than in the single rotated coordinates case shown in Table IV.

Inversion results are more meaningful when estimates of the uncertainties in the results are included. A qualitative estimate of the uncertainty in the results can be obtained by examining scatter plots of the cost function  $E$  versus the parameter values for all the states visited in the inversion in Figs. 15–18. In Fig. 15, the source parameters  $z_s$  (a),  $r_0$  (b), and  $\theta$  (c) have very small uncertainties, which is reasonable since they are the most sensitive parameters. The next most sensitive group of parameters,  $h_1$ ,  $\rho_1$ ,  $c_1$  [in Figs. 16(a)–(c)], and  $rc_2$  [in Fig. 17(c)] have reasonable distributions and relatively small uncertainties. Approximate upper bounds can be seen on the distributions for  $gc_1$  [in Fig. 16(d)],  $\alpha_{11}$ , and  $\alpha_{12}$  [in Figs. 18(a) and (b)]. The parameters for layer 2, other than  $rc_2$ , have very wide distributions in Figs. 17 and 18 indicating that, using the case 2 data, the cost function is not sensitive to changes in these parameter.

In summary, examples have been given to illustrate how the SDRC inversion method can obtain reliable estimates for the sensitive parameters in an efficient manner.

## IV. CONCLUSIONS

The SDRC inversion method has been introduced in this paper as a generalized, iterative inversion technique. The basic SDRC algorithm proceeds as follows. An initial set of rotated coordinates is calculated. A complete simulated annealing run is performed using the rotated coordinates with significant eigenvalues to compute the perturbations [Eq. (7)]. The bounds on the integration for the parameters represented in the primary eigenvectors are reduced. A new set of rotated coordinates is calculated, and another simulated annealing run is performed that begins at the parameter values obtained by the previous run. These steps are repeated until reasonable estimates have been found for the desired parameters.

Although the SDRC method is based on a rotated coordinates technique that has been reported previously, the work presented here is unique in several ways. The iterative SDRC algorithm is more efficient and able to find good estimates for more parameters than either standard annealing or a single rotated coordinates inversion. The ability of the SDRC method to obtain good estimates for the most sensitive parameters without accurate knowledge of the less sensitive parameters indicates that the SDRC method has the potential to be useful in real acoustic applications in which reliable estimates of the most sensitive parameters are needed very quickly.

The SDRC method has been introduced using the cost function in Eq. (3), ORCA,<sup>26</sup> a range-independent forward model, and a traditional representation of the source and environmental parameters. The SDRC method is a powerful general inversion technique that can be used with any cost function, forward model, or set of parameters. The SDRC method has also been applied to range-independent, experimental, broadband VLA data<sup>29</sup> and to simulated, range-dependent HLA data with added white Gaussian noise.<sup>30</sup>

## ACKNOWLEDGMENTS

This research was sponsored by the Office of Naval Research. The author wishes to thank Dr. David P. Knobles, Dr. Robert A. Koch, Dr. Brian R. LaCour, Dr. Ethan P. Honda, and Dr. Craig S. Macinnes for their helpful comments and discussions regarding this work and the reviewers for their insightful comments.

<sup>1</sup>A. Tolstoy, *Matched Field Processing for Underwater Acoustics* (World Scientific, New Jersey, 1993).

<sup>2</sup>E. K. Westwood, "Broadband matched-field source localization," *J. Acoust. Soc. Am.* **91**, 2777–2789 (1992).

<sup>3</sup>Section 3.8 of Ref. 1 contains a good summary of how environmental mismatch degrades MFP results.

<sup>4</sup>A. Tolstoy, N. R. Chapman, and G. Brooke, "Workshop '97: Benchmarking for geoaoustic inversion in shallow water," *J. Comput. Acoust.* **6**, 135–150 (1998).

<sup>5</sup>*Full Field Inversion Methods in Ocean and Seismo-Acoustics*, edited by O. Diachok, A. Caiti, P. Gerstoft, and H. Schmidt (Kluwer Academic, Dordrecht, The Netherlands, 1995).

<sup>6</sup>S. Kirkpatrick, C. D. Gelatt, Jr., and M. P. Vecchi, "Optimization by simulated annealing," *Science* **220**, 671–680 (1983).

<sup>7</sup>W. L. Goffe, G. D. Ferrier, and J. Rogers, "Global optimization of statistical functions with simulated annealing," *J. Econometr.* **60**, 65–99 (1994).

- <sup>8</sup>H. Szu and R. Hartley, "Fast simulated annealing," *Phys. Lett. A* **122**, 157–162 (1987).
- <sup>9</sup>P. Gerstoft, "Inversion of seismoacoustic data using genetic algorithms and a *posteriori* probability distributions," *J. Acoust. Soc. Am.* **95**, 770–782 (1994).
- <sup>10</sup>P. Gerstoft, "Inversion of acoustic data using a combination of genetic algorithms and the Gauss-Newton approach," *J. Acoust. Soc. Am.* **97**, 2181–2190 (1995).
- <sup>11</sup>M. R. Fallat and S. E. Dosso, "Geoacoustic inversion via local, global, and hybrid algorithms," *J. Acoust. Soc. Am.* **105**, 3219–3230 (1999).
- <sup>12</sup>M. R. Fallat, P. L. Nielsen, and S. E. Dosso, "Hybrid geoacoustic inversion of broadband Mediterranean Sea data," *J. Acoust. Soc. Am.* **107**, 1967–1977 (2000).
- <sup>13</sup>M. Haire, "Geoacoustic Inversion Using a Hybrid Optimization Algorithm," M. Sc. thesis, University of Texas at Austin, 2001.
- <sup>14</sup>While the author has not used genetic algorithms, one of the reviewers indicated that genetic algorithms are not affected by parameter correlations because the perturbations are not limited to the parameter axes.
- <sup>15</sup>M. D. Collins and L. Fishman, "Efficient navigation of parameter landscapes," *J. Acoust. Soc. Am.* **98**, 1637–1644 (1995).
- <sup>16</sup>R. J. Cederberg and M. D. Collins, "Application of an improved self-starter to geoacoustic inversion," *IEEE J. Ocean. Eng.* **22**, 102–109 (1997).
- <sup>17</sup>J. F. Lingeitch and M. D. Collins, "Estimating elastic sediment properties with the self-starter," *Wave Motion* **31**, 157–163 (2000).
- <sup>18</sup>J. S. Perkins, M. D. Collins, D. K. Dacol, L. T. Fialkowski, and J. F. Lingeitch, "Parameter coupling in broadband geoacoustic inversion," *J. Acoust. Soc. Am.* **109**, 2394 (2001).
- <sup>19</sup>L. Jaschke and N. R. Chapman, "Matched field inversion of broadband data using the freeze bath method," *J. Acoust. Soc. Am.* **106**, 1838–1851 (1999).
- <sup>20</sup>S. E. Dosso, "Quantifying uncertainty in geoacoustic inversion. I. A fast Gibbs sampler approach," *J. Acoust. Soc. Am.* **111**, 129–142 (2002).
- <sup>21</sup>S. E. Dosso and P. L. Nielsen, "Quantifying uncertainty in geoacoustic inversion II: Application to broadband, shallow-water data," *J. Acoust. Soc. Am.* **111**, 143–159 (2002).
- <sup>22</sup>D. P. Knobles and S. K. Mitchell, "Broadband localization by match-fields in range and bearing in shallow water," *J. Acoust. Soc. Am.* **96**, 1813–1829 (1994).
- <sup>23</sup>M. D. Collins and W. A. Kuperman, "Focalization: Environmental focusing and source localization," *J. Acoust. Soc. Am.* **90**, 1410–1422 (1991).
- <sup>24</sup>W. H. Press, A. Teukolsky, W. T. Vetterling, and B. P. Flannery, *Numerical Recipes in FORTRAN: The Art of Scientific Computing* (Cambridge University Press, Cambridge, 1992), Sec. 7.8.
- <sup>25</sup>E. L. Hamilton, "Geoacoustic modeling of the seafloor," *J. Acoust. Soc. Am.* **68**, 1313–1340 (1980).
- <sup>26</sup>E. K. Westwood, C. T. Tindle, and N. R. Chapman, "A normal mode model for acousto-elastic environments," *J. Acoust. Soc. Am.* **100**, 3631–3645 (1996).
- <sup>27</sup>D. P. Knobles, R. A. Koch, E. K. Westwood, and T. Udagawa, "The inversion of ocean waveguide parameters using a nonlinear least squares approach," *J. Comput. Acoust.* **6**, 83–97 (1998).
- <sup>28</sup>For the initial investigation discussed in this paper, the bound reduction was done manually. A systematic, automated bound reduction process is presented in Ref. 30.
- <sup>29</sup>T. B. Neilsen and D. P. Knobles, "A generalized inversion method: Simultaneous source localization and environmental inversion," *J. Acoust. Soc. Am.* **111**, 2388 (2002).
- <sup>30</sup>T. B. Neilsen and D. P. Knobles, "Geoacoustic inversion of range-dependent data with added Gaussian noise," submitted July 2002 to *IEEE J. Ocean. Eng. Special Issue on Geoacoustic Inversion in Range-Dependent Shallow-Water Environments*.